Journal of Cleaner Production 185 (2018) 357–365

Contents lists available at ScienceDirect

Journal of Cleaner Production

journal homepage: www.elsevier.com/locate/jclepro

Novel treatments for compatibility of plant fiber and starch by forming new hydrogen bonds

Chuan-Wei Zhang [a, b], Fang-Yi Li [a, b, *], Jian-Feng Li [a, b], Yan-Le Li [a, b], Jie Xu [a, b], Qi Xie [a, b], Shuai Chen [a, b], An-Fu Guo [c]

[a] Key Laboratory of High Efficiency and Clean Mechanical Manufacture (Ministry of Education), School of Mechanical Engineering, Shandong University, Jinan 250061, China
[b] National Demonstration Center for Experimental Mechanical Engineering Education, Shandong University, Jinan 250061, China
[c] School of Mechanical & Automobile Engineering, Liaocheng University, Liaocheng 252059, China

ARTICLE INFO

Article history:
Received 13 July 2017
Received in revised form
24 February 2018
Accepted 1 March 2018
Available online 1 March 2018

Keywords:
Biodegradable composite
Plant fiber
Starch
Compatibility
Hydrogen bond

ABSTRACT

Cross-reaction of oxidization and plasticization was employed to prepare thermoplastic oxidized starch (TPOS). Oxidized ureal plant fiber (OUF) was prepared by soaking the plant fiber in H_2O_2 and treating it with urea at low temperature (−15 °C). X-ray diffraction analysis showed that the crystallinity index of TPOS decreased from 19.95% to 0.89%. Amorphous starch more easily combined with the plant fiber. Moreover, infrared spectrum analysis indicated that the O—H stretching vibration peak of the TPOS/OUF composite moved to 3375.4 cm^{-1} from 3414.0 cm^{-1}, which revealed that new hydrogen bonds were formed in the TPOS/OUF composite. The H atoms of the O—H groups in starch and plant fiber were oxidized to highly polar H^+. The N atoms in urea and O atoms in glycerol got quite close to these highly polar H^+ groups and experienced an unusually strong field, which are known as hydrogen bonds. The newly formed hydrogen bonds made the plant fiber compatible with starch. Compatibility was experimentally validated by microscopic observation. For industrial application, new green composites and products were prepared using the TPOS/OUF composite slurry through a pollution-free process.

1. Introduction

Petroleum-based materials, such as polystyrene and polyethylene, occupy a massive portion of the waste worldwide. The lack of biodegradability leads to a large environmental problem (Wilcox et al., 2015; Madadian et al., 2017). In light of global concern for the accumulation of wastes, researchers focused considerable interest on developing biodegradable and compostable materials to partially replace petroleum-based plastics (Thakur et al., 2014; Khan et al., 2010). Natural plant fiber is a cheap and renewable resource that is abundantly available in nature. Global productions of agricultural plant fiber from corn straw, wheat straw, coconut, sisal fiber, and sugarcane bagasse were estimated to be at 1.4 billion tons (Saini et al., 2015; Jawaid and Abdul Khalil, 2011). These residual plant fibers are available for use in value-added composites. Researchers used plant fibers along with polymers, such as polypropylene, epoxy, vinyl, resin, polyester, and starch, to produce biodegradable hybrid composites (Akil et al., 2011; Sekhar, 2017). Furthermore, starch is one of the most abundant renewable biopolymers (Zhang et al., 2017; Vroman and Tighzert, 2009). As recent focus of research, starch is suitable for the production of green composites in combination with plant fiber.

Starch is found in nature in semi-crystalline granule form. Depending on the botanical source, the degree of crystallinity of starch varies from 20% to 45% (Jenkins and Donald, 1995, 1996). Native starch displays high water sensitivity and low mechanical strength. Notably, starch can be plasticized to some degree with plasticizers, such as water, amides, polyols, and ionic liquids (Wilpiszewska and Spychaj, 2011; Ma et al., 2010). However, some shortcomings of thermoplastic starch (TPS), such as induced brittleness and plasticizer leaching, limit its applications. To overcome several of these problems, TPS has been modified using physical and chemical modifications, including graft copolymerization (Jyothi, 2010), etherification (Maubane et al., 2017), oxidization (Yang et al., 2010), and esterification (Adak and Banerjee, 2016).

* Corresponding author. Key Laboratory of High Efficiency and Clean Mechanical Manufacture (Ministry of Education), School of Mechanical Engineering, Shandong University, Jinan 250061, China.
E-mail address: lifangyi@sdu.edu.cn (F.-Y. Li).

https://doi.org/10.1016/j.jclepro.2018.03.001
0959-6526/

Optimum hybridization results of fiber-reinforced composites are acquired when the fibers are highly strain compatible with polymers (Nunna et al., 2012). Starch and plant fibers are both polysaccharides and possess a similar chemical composition. However, both polysaccharides are composed mostly of polar molecules, and plant fibers are poorly compatible with starch (Wattanakornsiri and Tongnunui, 2014; Müller et al., 2014). The modification of fibers reportedly improves adhesion and the final mechanical properties of the starch/plant fiber composites (Satyanarayana et al., 2009; Rosa et al., 2009). Other different chemical modifications on natural fibers for use in natural fiber-reinforced composites were discussed. These modifications include alkalization, silane treatment, acetylation, benzoylation, acrylation, the use of maleated coupling agents, and plasma treatment (http://xueshu.baidu.com/s?wd=author%3A%28de%20Farias%20JG%29%20&tn=SE_baiduxueshu_c1gjeupa&ie=utf-8&sc_f_para=sc_hilight%3Dperson; Li et al., 2007; http://xueshu.baidu.com/s?wd=author%3A%28de%20Farias%20JG%29%20&tn=SE_baiduxueshu_c1gjeupa&ie=utf-8&sc_f_para=sc_hilight%3Dperson; Farias et al., 2017). The incompatibility of starch and plant fibers is a bottleneck problem that restricts the preparation and mechanical properties of composites combining starch and plant fiber. The compatibility of plant fiber and starch is not fully achieved yet.

In this work, novel treatments of starch and plant fiber were developed to improve their compatibility. Cross-reaction with oxidization and plasticization was used to modify starch, preparing thermoplastic oxidized starch (TPOS). Sisal fiber was soaked in hydrogen peroxide solution and then treated with urea at low temperature (−15 °C) to prepare oxidized ureal plant fiber (OUF). New hydrogen bonds were formed between TPOS and OUF. The new hydrogen bonds caused the plant fiber to bind with starch tightly to form a homogeneous phase, resulting in the compatibility of plant fiber with starch.

The sequence of events following crystallinity, chemical groups, and microstructure of TPOS, OUF, and TPOS/OUF composites were investigated using X-ray diffraction, infrared spectrum analysis, and atomic force microscopy (AFM) to obtain a comprehensive view on the compatibility mechanism of starch and plant fiber. Compatibility was experimentally validated by microscopic observation of the TPOS/OUF composite slurry. Biodegradable products for industrial applications were prepared through foam molding process using the TPOS/OUF composite slurry as raw materials.

2. Materials and methods

2.1. Materials

Sisal fiber, with an average length of 5 mm and an average diameter close to 60 μm, determined using optic microscopy, was prepared in our laboratory. The amylose content of corn starch is about 26.2%, determined using dual-wavelength spectrophotometry method (Shi et al., 2011), which was purchased from Hebei Huachen Starch Sugar Co., Ltd. (Hebei, China). Glycerol, which was used as plasticizing agent, was purchased from Tianjin Fuyu Fine Chemical Co., Ltd. (Tianjin, China). Hydroxyl peroxide with analytical grade (99.5%) as oxidizing agent was purchased from Chengdu Kelong Chemical Reagent Co., Ltd. (Sichuan, China). Urea was purchased from Yantai Shuangshuang Chemical Co., Ltd. (Shandong, China). Expandable polyethylene (EPE) was purchased from Qingdao Zhonglong Technology Co., Ltd. (Shandong, China). Expanded polystyrene (EPS) was purchased from Langfang Yumei Lagging Material Co., Ltd. (Hebei, China). The corrugated board was purchased from Yuanyuan Packaging Material Co., Ltd. (Guangdong, China).

2.2. Preparation of the TPOS

TPOS was prepared as follows. In total, 200.0 mL distilled water and 40.0 g native starch (NS) were combined in a 500 mL round-bottomed cup, and the mixture was heated at 80 °C for 30 min with mild stirring to prepare gelatinized starch. Then, 25 mL distilled water was added to the mixture with 10 mL of H_2O_2 after the temperature decreased to 25 °C. During oxidation, the mixture was vigorously stirred mechanically for 1 h to ensure that the H_2O_2 was uniformly dispersed in the gelatinized starch. Afterward, glycerol and oxidized starch at the mass proportion (glycerol/oxidized starch) of 1/10 were mixed under high-speed stirring and maintained in a water bath at 80 °C for 2 h to prepare TPOS (Zhang et al., 2017).

2.3. Preparation of OUF

OUF was prepared as follows. The sisal fiber was cut into a 6 mm-long fiber. H_2O_2 solution (10.0 mL) and distilled water (100.0 mL) were mixed in a 500 mL round-bottomed cup. Then, 10 g of native sisal fiber (NF) was soaked in the mixture solution at 25 °C for 12 h to prepare oxidized fiber. Afterward, the oxidized fibers were treated with urea at low temperature (−15 °C) for 8 h to prepare OUF (Cai and Zhang, 2005). TPOS and OUF were mixed for 30 min to prepare the TPOS/OUF composite. The total technological preparation process of TPOS, OUF, and the TPOS/OUF composite slurry is shown in Fig. 1.

2.4. X-ray diffraction experiment

The TPOS was dried at 100 °C for 24 h to remove moisture. Then, the anhydrous TPOS was ground using an agate mortar and filtered using a 200-mesh sieve. The compacted sample was flat, and its surface was parallel with the glass frame. The assay was operated at room temperature by using Ni-filtered Cu radiation and a curved graphite crystal monochromator. The slit system was DS/RS/SS = 1°/0.16 mm/1°. The angle (2θ) interval of 5°–75° was analyzed at a speed of 5 °C min^{-1}.

2.5. AFM investigation

AFM studies were conducted using a thermal microscope combined AFM/SNOM system. Sections were scanned in air by using the dry scanner attachment. Samples were scanned in the direct-current contact mode and recorded as topographical and error signal mode images. SiN_3 cantilevers were used with a nominal force constant of 0.38 nm^{-1}. Scan sizes ranged from 1 μm to 100 μm. The scan rate was between 2.0 and 2.5 Hz.

2.6. Infrared spectrum analysis

OUF and the composites were dried at a constant temperature of 100 °C for 24 h to remove moisture. Approximately 1 mg of the powder was mixed with 150 mg of KBr and milled thoroughly until the particle diameter was less than 2.5 μm. This mixture was compressed into pellets under a pressure of 12–14 MPa and then analyzed using the VERTEX 70 fourier transform infrared spectrometer (FTIR). The spectra were recorded with a resolution of 2 cm^{-1} in the range of 400–4000 cm^{-1}.

3. Industrial application and products

3.1. Preparation of the composites and products

Given their mass and energy transport, acoustic absorption,

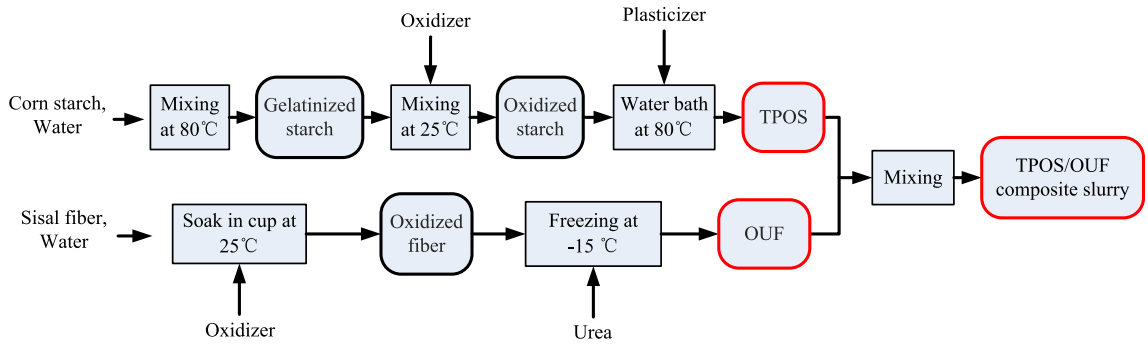

Fig. 1. Technological process flowchart of TPOS, OUF, and TPOS/OUF composite slurry.

light weight, and cushioning properties, synthetic composites with open cell structures are used in a multitude of different applications, including packaging and transportation (Lee and Park, 2000; Naguib et al., 2002). In this work, a new biodegradable composite with open cells was prepared using the TPOS/OUF composite slurry as raw materials. The composite preparation included two phases: slurry preparation and foaming process. Fig. 1 illustrates the first step. The TPOS/OUF composite slurry was prepared. Then, other additive agents were added to the slurry to prepare the composites. The ingredients of the composites are shown in Table 1. Talcum powder was the filling agent, which did not react with other additives. Azodicarbonamide, the foaming agent, decomposed at 195 °C–210 °C and consequently produced nitrogen and carbon dioxide. Subsequently, the prepared slurry was injected into the compression foam molding machine, as shown in Fig. 2. The upper and lower molds were closed to shape the slurry. After 10 s, the upper molds were raised to a certain height to create a foaming area above the slurry. After the decomposition of the foaming agent in the slurry, gas was released toward the foaming area. The foaming area pressure was controlled at 2.5–3.0 MPa by using a pressure transducer and gas metering valve, whereas the temperature was maintained at 195 °C–205 °C. After 2 min, the upper and lower molds were opened. The biodegradable composites were prepared. The whole process was formed at one time, no other machining was needed, and no other waste was discharged except a large amount of water vapor and a small amount of nitrogen.

The images of the biodegradable composites and its internal structure are presented in Fig. 3. The thickness of the composites was 5 mm. The interior of the composites was filled with open cells. As a result of their open cell structure, the composites exhibit excellent insulation and mechanical properties. Therefore, the composites can be used in many applications, including packaging and indoor decorations. Fig. 4 presents a kind of product of the composites: mobile phone packing box.

3.2. Compressive and tensile strength tests

For the compressive strength experiment, test samples ($100 \times 100 \times 25\ mm^3$) were prepared according to GB/T 8168-2008 China. Using the standard method, the XYD-15 K compression testing machine was preloaded with 5 kN of specimens. The thickness of the specimens was regarded as original thickness. The tensile strength experiments were performed according to GB/T 9641-88 China. Test samples ($100 \times 100 \times 5\ mm^3$) were prepared. All measurements were conducted on five specimens, and average results were taken. Four kinds of materials were tested, namely, EPE, EPS, corrugated board, and the composites prepared earlier.

Table 1
The composite components.

Material	OUF	TPOS	Water	Talcum powder	Azodicarbonamide
Mass (g)	100	60	250	25	2

4. Results and discussions

4.1. Crystal structure analysis of TPOS and NS

Fig. 5 shows the recorded X-ray diffractograms patterns of NS, TPS, and TPOS. Results demonstrated important changes in the structure of the starch after plasticization. Diffraction peaks of NS were located at $2\theta = 15.5°$, 18.2°, 23.4°. NS analysis displayed a predominance of crystallinity type A. NS can be gelatinized when mixed in hot water, and the crystal structures of starch were destroyed. However, the starch will achieve retrogradation when water is lost and the temperature decreases (Morales et al., 2015). A crystal diffractogram peak was found in the X-ray diffractogram of TPS. TPS diffraction peak was located at $2\theta = 19.8°$, 22.3°. The formation of B– and V-type crystal structures occurred in TPS while the starch was in gelatin form because of recrystallization. By fitting the calculation using Jade software, the computed NS crystallinity index was 19.95%, and the TPS crystallinity index was 14.3%. Significantly, diffraction peaks were not found in the X-ray diffractogram of TPOS, which exhibited a crystallinity index of 0.89%. These findings demonstrated that the crystal state observed in the NS granules was completely destroyed in TPOS. The structure of starch crystallization was eliminated, and amorphous starch was increased. Amorphous starch more easily combined with plant fibers, leading to a more uniform blend of plant fiber and starch.

4.2. Microstructure of TPOS and NS

AFM images of TPOS and NS are shown in Fig. 6. Force modulation imaging generates contrast that depends on the relative stiffness of different regions of the sample. Harder regions appear brighter in the images (Ridout et al., 2003). The force modulation images of NS and TPOS are shown in Fig. 6 (b, d). The interconnecting matrix that appeared bright relative to the blocks suggested that this matrix region was stiffer and potentially exhibited more crystal structures than other regions. More matrix regions were observed in the force modulation image of NS (Fig. 6 (b)) than that in the force modulation of TPOS (Fig. 6 (d)). This finding indicated that plasticization destroyed the crystal structure of starch, consistent with the test results of the crystal structure analysis in Fig. 5. Internal embossment structures were clearly defined in the AFM images (Ridout et al., 2002). The error signal mode images showed integrated embossment structure, and the embossment was clear in the NS image (Fig. 6 (a)); however, the

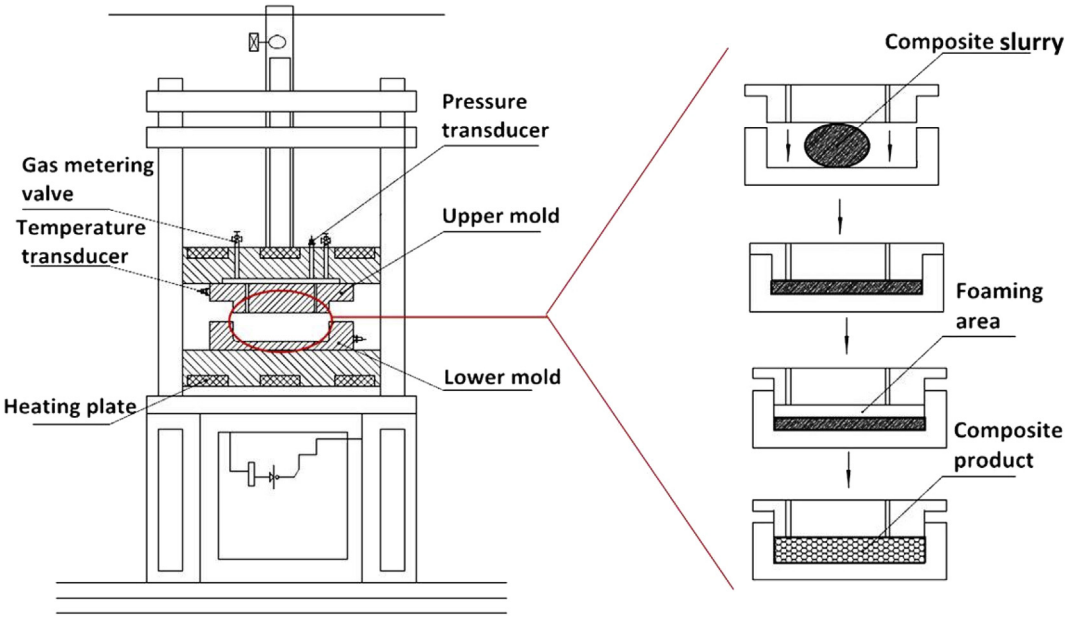

Fig. 2. Diagram of the foam molding machine.

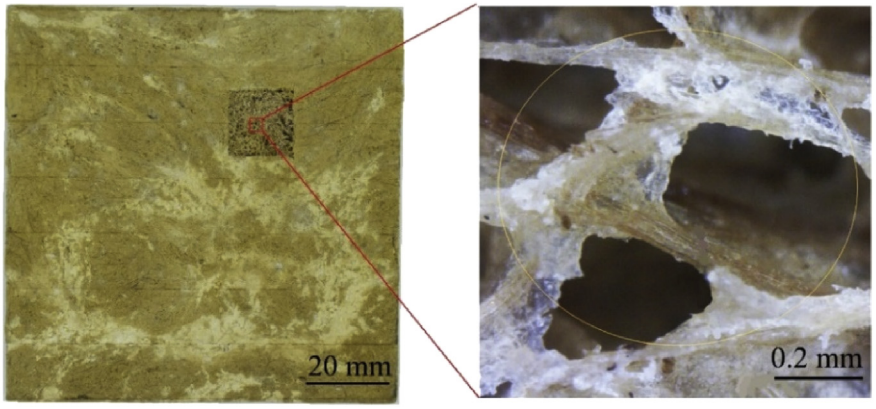

Fig. 3. Images of the composite with fully open cell structures.

Fig. 4. A product of the composite.

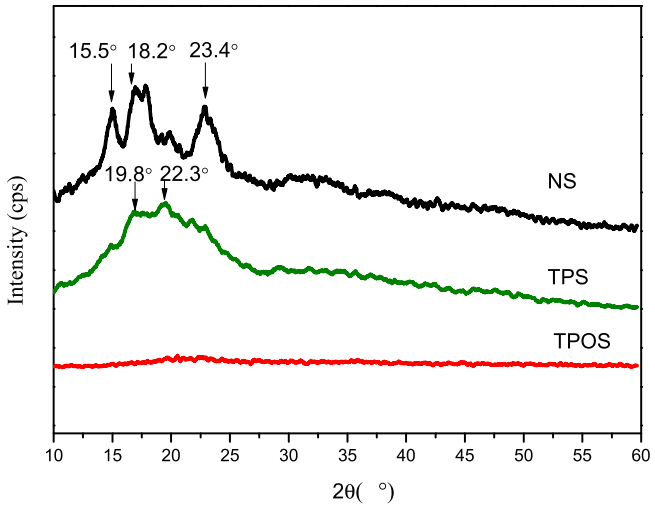

Fig. 5. X-ray diffractograms of NS, TPS, and TPOS.

embossment structures became less and chaotic in the TPOS image (Fig. 6 (c)). The result showed that the NS molecules were gathered; by contrast, the starch molecules in TPOS were uniformly distributed, and the amorphous starch section was enlarged.

4.3. Formation of new hydrogen bonds between TPOS and OUF

A large amount of hydrogen bonds H–O···H are present between the O–H groups in carbohydrate polymers, such as starch and plant fiber (Pfister and Zeeman, 2016). The infrared spectra of NF and OUF are shown in Fig. 7. The spectra were concentrated on the following characteristic bands: 3570–3050 cm^{-1}, which was related to the stretching of the O–H groups in polysaccharides, and 1100–3050 cm^{-1}, which corresponded to the stretching of C–OH in polysaccharides. In comparison with the above stretching bonds of NF and OUF, the peak related to the hydroxyl groups of OUF was evidently lower, demonstrating that the hydroxyl group stretching was weakened after oxidization and urea treatment.

The "hydrogen bonding effect" indicates that the O–H stretching vibration wavenumber of the infrared spectrum moves to a lower value when the O–H groups form new hydrogen bonds. The formation of stronger hydrogen bonds between the O–H groups results in increased stretching vibration wavenumber shifts to a lower level (Finch, 1970).

According to the harmonic oscillator model, the reduction in force constant Δf can be represented by Equations (1) and (2) (Naka et al., 1998; Pawlak and Mucha, 2003):

$$\Delta f = f_p - f_{np} = \frac{\mu\left(v_{np}^2 - v_p^2\right)}{4\pi^2}. \quad (1)$$

$$\mu = \frac{m_1 m_2}{m_1 + m_2} = \frac{M_1 M_2}{M_1 + M_2}. \quad (2)$$

where μ corresponds to the reduced mass of the oscillator, m_1 and m_2 are the masses of the chemical-bonded atoms, $M_1$and M_2 are the relative atomic masses, N_A is Avogadro's constant, f is the force constant, and v is the oscillating frequency. The subscripts m and nm denote modified and nonmodified oscillators, respectively. Some interactions are directly related to the frequency shift of stretching vibrations and lead to the reduction of force constant. The hydrogen-bonding effect obviously changes the oscillating frequencies of the O–H groups in the infrared spectrum, which

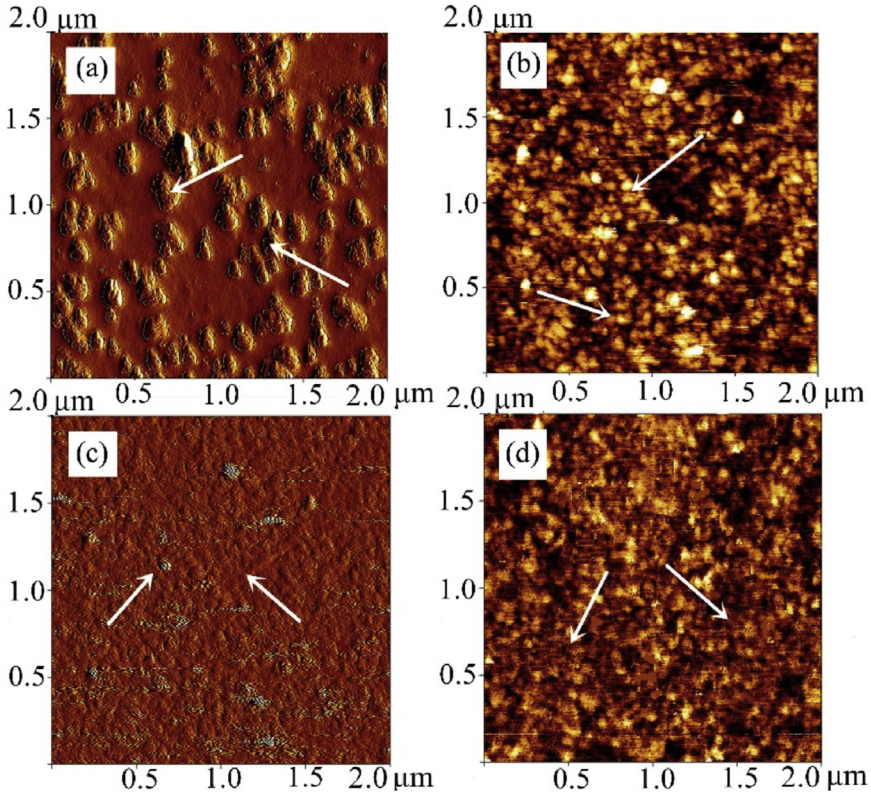

Fig. 6. AFM images of starch: error signal mode images of NS (a) and TPOS (c); force modulation images of NS (b) and TPOS (d).

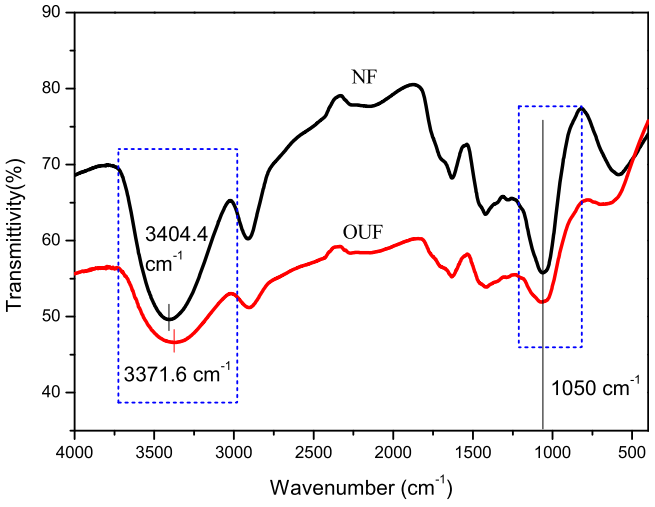

Fig. 7. Infrared spectra of NF and OUF.

drives the absorbance to move toward the lower frequency. The frequency equals the wavenumber times the speed of light. The more the wavenumber moves, the more the $\triangle f$ changes, and the stronger the hydrogen bonds are formed (Xu et al., 2000).

Fig. 7 shows that the oxidization and urea treatment of plant fiber led to a significant reduction in wavenumber from 3404.4 cm^{-1}–3371.6 cm^{-1}, revealing that new hydrogen bonds were formed in OUF. Fig. 8 illustrates the changes in the wavenumber and absorbance in the region of the O—H group vibrations of the composites. Absorption peaks of the O—H groups in the TPOS/OUF composite moved to a lower wavenumber (3375.4 cm^{-1}), compared with those of the TPOS/NF composite (3414.0 cm^{-1}). According to Equations (1) and (2), Δf was calculated in Table 2. The Δf of TPOS/NF composite and TPOS/OUF composite was larger than that of NF and OUF. Larger Δf reveals that new hydrogen bonds formed between the TPOS and OUF.

The details of the hydrogen bonding are presented in the molecular model of the TPOS and OUF combination in Fig. 9. Strong oxidization of H_2O_2 transferred the electrons of H from NF molecules to the oxidizer, forming a highly polarized H^+ in the O—H group. Considering that the electron-depleted H atom possessed a particularly small size, thus, other electronegative atoms, such as

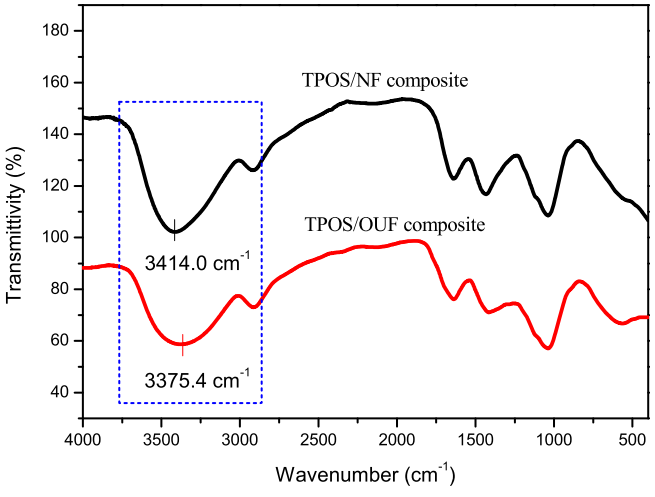

Fig. 8. Infrared spectra of TPOS/NF composite and TPOS/OUF composite.

Table 2
Wavenumber of O—H groups in FTIR spectrum and the change of force (Δf).

Materials	Wavenumber peak of O—H groups (cm^{-1})	Force constant (Δf) (10^{-18}N)
NF	3404.4	2.64
OUF	3371.6	
TPOS/NF composite	3414.0	3.13
TPOS/OUF composite	3375.4	

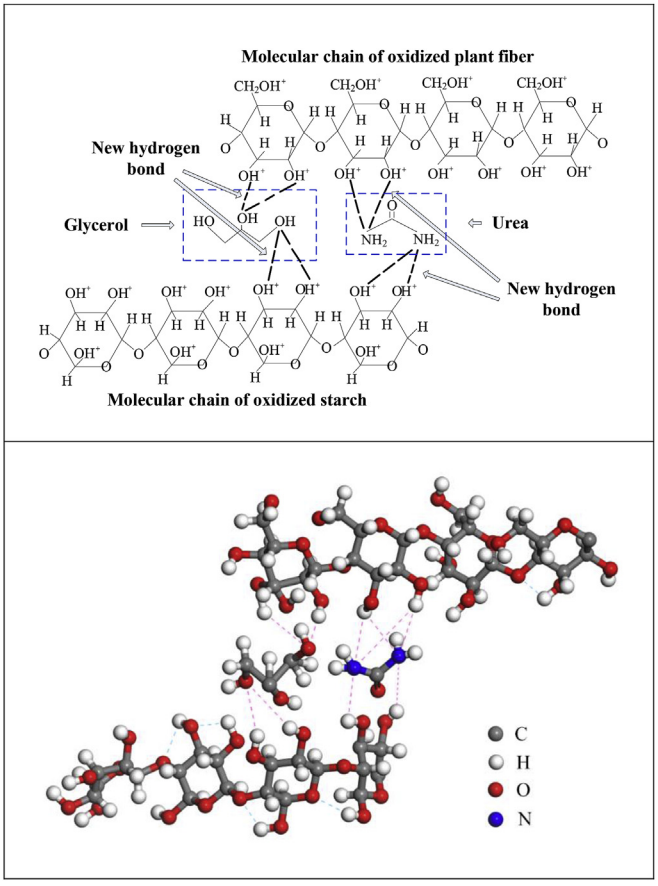

Fig. 9. Molecular model of TPOS and OUF combination by new hydrogen bonds.

the N atoms in urea, approached these highly polar H^+ groups and experienced an unusually strong field. The resulting bonds are known as hydrogen bonds, which are depicted by X—···H^+ (Israelachvili, 2011). The fiber and urea molecules formed hydrogen bonds in the OUF. Moreover, H_2O_2 caused the H atoms of the O—H group in the starch molecule to lose electrons. The H atoms in starch were oxidized to highly polar H^+. Electronegative atoms, O atoms in the plasticizer (glycerol), formed hydrogen bonds with polar H^+ of the starch in TPOS. When OUF mixed with TPOS, new hydrogen bonds formed between glycerol and fiber molecules; moreover, urea bonded with starch through the new hydrogen bonds. Therefore, urea and glycerol functioned as bridges, and new hydrogen bonds formed between OUF and TPOS.

4.4. Compatibility of TPOS and OUF

Compatibility was experimentally validated using a microscope to observe the combination images of plant fiber and starch, as shown in Fig. 10. TPOS tightly combined with NF, as shown in Fig. 10 (a, b). However, a distinct interface was observed between sisal

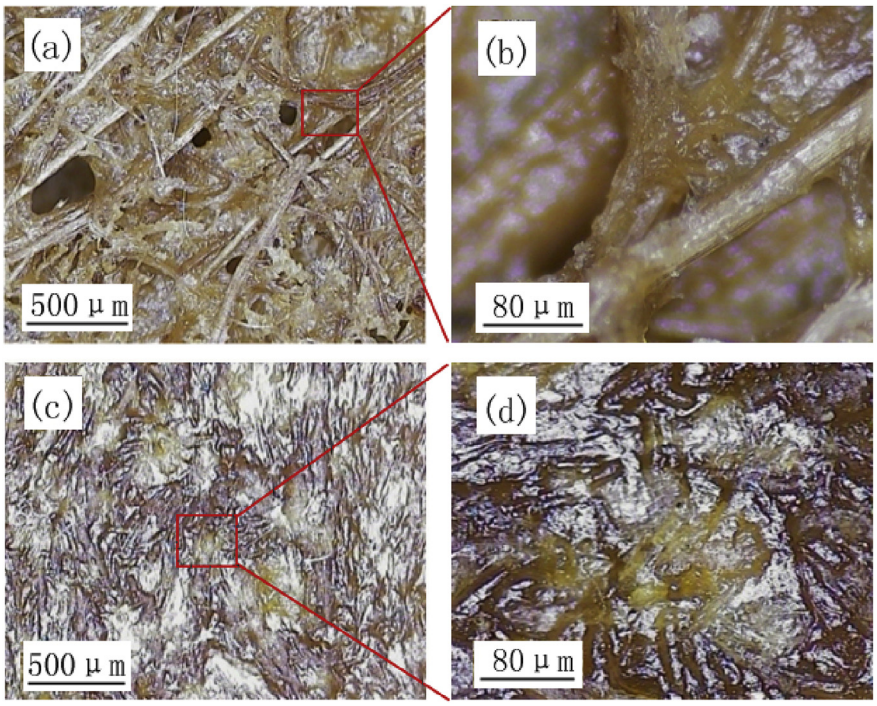

Fig. 10. Combination images of sisal fiber and corn starch: TPOS/NF composite (a, b), TPOS/OUF composite (c, d).

fiber and TPOS, and starch and fiber agglomerated independently. Evidently, pant fiber and starch are poorly compatible. Fig. 10 (c, d) shows the combination of OUF and TPOS. After oxidization and urea treatment at low temperature, sisal fiber was homogeneously dispersed in TPOS, similar to jelly. This outcome showed that plant fiber and starch were compatible in the OUF/TPOS composite slurry. The changes in the molecular structure of starch after plasticization and plant fiber after oxidization-urea treatment formed new hydrogen bonds between TPOS and OUF.

The new hydrogen bonds tightly bound plant fiber to starch to form a homogeneous phase. This outcome explained the phenomenon in which plant fiber and starch became compatible. To verify the feasibility of the above method, bagasse fiber was also selected for the preparation of OUF. The combination images of bagasse fiber and starch are presented in Fig. 11. The same results were obtained, that is, excellent compatibility was observed between OUF and TPOS.

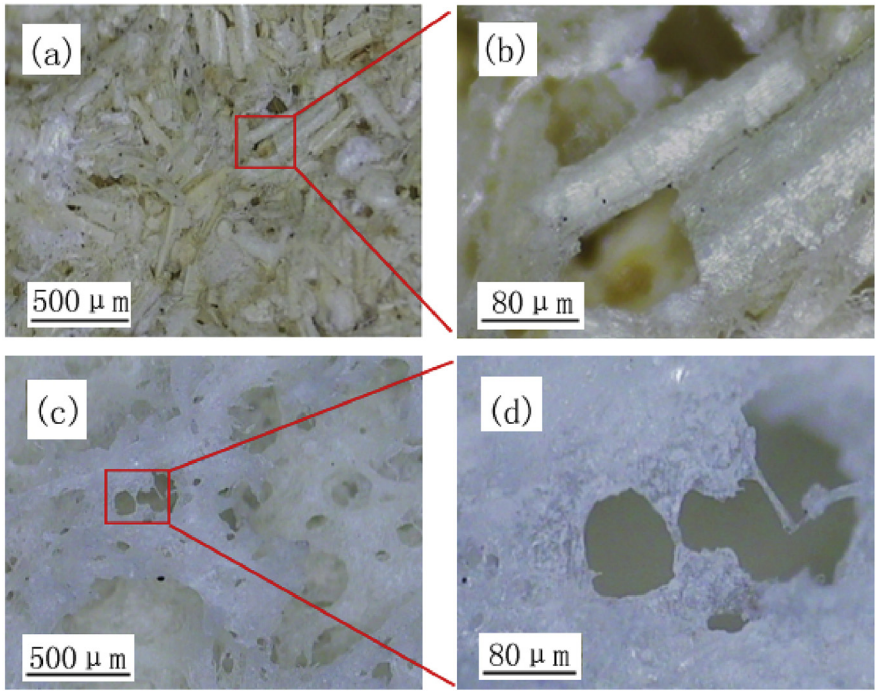

Fig. 11. Combination images of bagasse fiber and corn starch: TPOS/NF composite (a, b), TPOS/OUF composite (c, d).

4.5. Industrial application analysis of the composites

Compressive and tensile strengths of EPS, EPE, corrugated board, and the composites were investigated, and results are shown in Fig. 12. Results indicated that the tensile strength of the composites was 4.17 MPa, and the compressive strength was 5.32 MPa. Obviously, the mechanical properties of the composites were better than those of EPS, EPE, and corrugated board. EPE and EPS are plastic products that are non-biodegradable. Plastic materials are widely used in industrial packaging, which causes accumulation of waste. Corrugated board is another packaging material, which can be degraded. However, the production process of the corrugated paperboard discharges large amounts of wastewater, which leads to serious environment pollution. The new composites with excellent mechanical properties are green and sustainable. The raw materials are renewable, the production process is pollution-free, and the products are biodegradable.

In order to obtain environmental effect of the composite, the life cycle environmental impacts of the composite were quantitatively analyzed by using Eco-indicator 99 life cycle evaluation method (Siracusa et al., 2014). The environmental impact of the composite was evaluated and analyzed by SimaPro7 that is a special software for life cycle evaluation. Moreover, the environmental impacts of the composite and other typical packaging materials were analyzed and compared, as shown in Table 3. The composite showed the lowest impact on human health, ecological environment and resource consumption in the whole life cycle assessment. It shows that the composites are environment-friendly materials. In addition, the production costs of the typical packaging materials were investigated and analyzed, by using these materials to produce one mobile phone package as an example. The mobile phone packing box on the market are produced using fine cardboard and plastic materials, at a production cost of $0.07 per mobile phone package. The cost of producing the same mobile phone package using the new composite was calculated. The cost of one product is $0.03 including raw material cost, energy cost, labor cost and equipment depreciation cost. The detailed calculation processes of the composite costs and life cycle environmental impacts are shown in the supplementary material. Therefore, the application of the new composite to industrial production has good economic and environmental benefits. The new composite is an ideal alternative as packaging material.

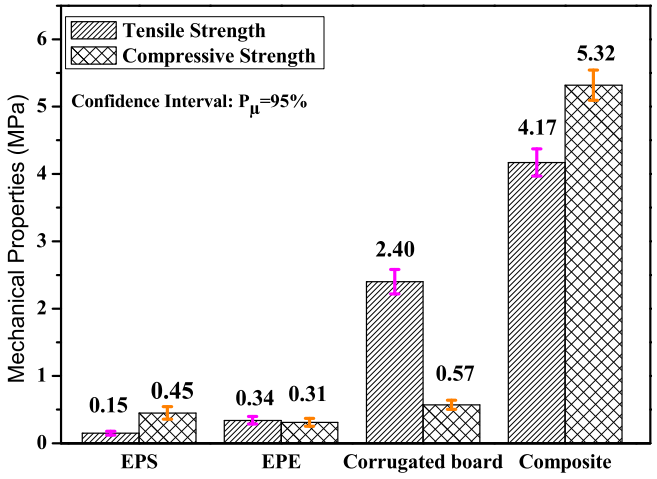

Fig. 12. Mechanical properties of EPS, EPE, corrugated board and the composite.

Table 3
Life cycle assessment results of typical packaging materials.

Types	EPS	EPE	Corrugated board	Composite
Human health	0.151 Pt	0.053 Pt	0.0404 Pt	0.0162 Pt
Ecosystem quality	0.299 Pt	0.118 Pt	0.0889 Pt	0.0030 Pt
Resources	0.352 Pt	0.252 Pt	0.0551 Pt	0.0341 Pt
Total	0.802 Pt	0.423 Pt	0.184 Pt	0.053 Pt

5. Conclusions

Starch is one of the most abundant renewable biopolymers. In this study, starch was combined with plant fiber to prepare new green composites. The incompatibility of starch and plant fibers was a bottleneck that restricted the preparation and mechanical properties of the composites. In this paper, plant fiber showed good compatibility with starch by employing novel treatments of starch and plant fiber.

Cross-reaction with oxidization and plasticization was used to prepare TPOS. The X-ray diffraction analysis showed that crystallization was eliminated in TPOS. The crystallinity index of NS was 19.95%. The crystallinity index of TPOS decreased to 0.89% from 19.95%. Amorphous starch easily combined with plant fiber.

Sisal fiber was soaked in hydrogen peroxide solution and then treated with urea at low temperature (−15 °C) to prepare OUF. Infrared spectrum analysis indicated that the O—H stretching vibration peak evidently weakened in OUF. In addition, the O—H stretching vibration peak wavenumber of OUF moved to lower values (3404.4 cm^{-1}) compared with that of NF (3371.6 cm^{-1}), revealing that new hydrogen bonds were formed in OUF.

H_2O_2 caused the H atoms of the O—H group in the starch and plant fiber molecule to lose electrons. The H atoms were oxidized to highly polar H^+. Electronegative atoms, such as N atoms in urea and O atoms in glycerol, closely approached these highly polar H^+ groups and experienced an unusually strong field. The resulting bonds are known as hydrogen bonds. With urea and glycerol as bridges, new hydrogen bonds formed between OUF and TPOS, as verified by infrared spectrum analysis of the TPOS/OUF composite.

The newly formed hydrogen bonds tightly bound plant fiber to starch to form a homogeneous phase, resulting in the compatibility of plant fiber with starch. Compatibility was experimentally validated by observing the combination images of the OUF/TPOS composites.

A new composite with open cell structures was prepared by foam molding by using the TPOS/OUF composite slurry. The composite exhibited excellent mechanical properties, great environmental and economic effects. Therefore, the composite is a potential alternative as packaging material.

Acknowledgements

This work was financially supported by National Natural Science Foundation of China (No.51775318) and China Postdoctoral Science Foundation (No.2016M592180). We would like to thank our colleagues from Shandong University.

Appendix A. Supplementary data

Supplementary data related to this article can be found at https://doi.org/10.1016/j.jclepro.2018.03.001.

References

Adak, S., Banerjee, R., 2016. A green approach for starch modification: esterification by lipase and novel imidazolium surfactant. Carbohydr. Polym. 150, 359.
Akil, H.M., Omar, M.F., Mazuki, A.A.M., Safiee, S., Ishak, Z.A.M., Bakar, A.A., 2011.

Kenaf fiber reinforced composites: a review. Mater. Des. 32 (8–9), 4107–4121.
Cai, J., Zhang, L., 2005. Rapid dissolution of cellulose in LiOH/urea and NaOH/urea aqueous solutions. Macromol. Biosci. 5 (6), 539–548.
Finch, A., 1970. Chemical Applications of Far Infrared Spectroscopy. Academic Press.
Farias, J.G., de Cavalcante, R.C., Canabarro, B.R., Viana, H.M., Scholz, S., Simão, R.A., 2017. Surface lignin removal on coir fibers by plasma treatment for improved adhesion in thermoplastic starch composites. Carbohydr. Polym. 165, 429.
Israelachvili, J.N., 2011. Intermolecular and surface forces-intermolecular and surface forces (third edition). QRB (Q. Rev. Biol.) 2 (3), 59–65.
Jawaid, M., Abdul Khalil, H.P.S., 2011. Cellulosic/synthetic fibre reinforced polymer hybrid composites: a review. Carbohydr. Polym. 86, 1–18.
Jenkins, P.J., Donald, A.M., 1995. The influence of amylose on starch granule structure. Int. J. Biol. Macromol. 17 (6), 315–321.
Jenkins, P.J., Donald, A.M., 1996. Application of small-angle neutron scattering to the study of the structure of starch granules. Polymer 37 (25), 5559–5568.
Jyothi, A.N., 2010. Starch graft copolymers: novel applications in industry. Compos. Interfac. 17 (2–3), 165–174.
Khan, J.A., Khan, M.A., Islam, R., Gafur, A., 2010. Mechanical, thermal and interfacial properties of jute fabric-reinforced polypropylene composites: effect of potassium dichromate. Mater. Sci. Appl. 1, 350–357.
Lee, S.T., Park, C.B., 2000. Foam Extrusion - Principles and Practice. Crc Press.
Li, X., Tabil, L.G., Panigrahi, S., 2007. Chemical treatments of natural fiber for use in natural fiber-reinforced composites: a review. J. Polym. Environ. 15 (1), 25–33.
Ma, X., Yu, J., Jin, F., 2010. Urea and formamide as a mixed plasticizer for thermoplastic starch. J. Appl. Polym. Sci. 93 (4), 1769–1773.
Madadian, E., Crowe, C., Lefsrud, M., 2017. Evaluation of composite fiber-plastics biomass clinkering under the gasification conditions. J. Clean. Prod. 164, 137–145.
Maubane, L., Ray, S., Jalama, K., 2017. The effect of starch amylose content on the morphology and properties of melt-processed butyl-etherified starch/poly [(butylene succinate)-co-adipate] blends. Carbohydr. Polym. 155, 89–100.
Morales, N.J., Candal, R., Famá, L., Goyanes, S., Rubiolo, G., 2015. Improving the physical properties of starch using a new kind of water dispersible nano-hybrid reinforcement. Carbohydr. Polym. 127, 291–299.
Müller, P., Renner, K., Móczó, J., Fekete, E., Pukánskzy, B., 2014. Thermoplastic starch/wood composites: interfacial interactions and functional properties. Carbohydr. Polym. 102, 821–829.
Naguib, H.E., Park, C.B., Panzer, U., Reichelt, N., 2002. Strategies for achieving ultra low-density polypropylene foams. Polym. Eng. Sci. 42 (7), 1481–1492.
Naka, K., Nakamura, T.O.A., Maeda, S., Aoi, K., Takasu, A.O.M., Yamashita, R., 1998. Chitin-graft-poly(2-methyl-2-oxazoline) enhanced solubility and activity of catalase in organic solvent. Int. J. Biol. Macromol. 23 (4), 259–262.
Nunna, S., Chandra, P.R., Shrivastava, S., Jalan, A.K., 2012. A review on mechanical behavior of natural fiber based hybrid composites. J. Reinforc. Plast. Compos. 31 (11), 759–769.
Pawlak, A., Mucha, M., 2003. Thermogravimetric and FTIR studies of chitosan blends. Thermochim. Acta 396 (1–2), 153–166.
Pfister, B., Zeeman, S.C., 2016. Formation of starch in plant cells. Cell. Mol. Life Sci. 73 (14), 2781–2807.
Ridout, M.J., Gunning, A.P., Parker, M.L., Wilson, R.H., Morris, V.J., 2002. Using AFM to image the internal structure of starch granules. Carbohydr. Polym. 50 (2), 123–132.
Ridout, M.J., Parker, M.L., Hedley, C.L., Bogracheva, T.Y., Morris, V.J., 2003. Atomic force microscopy of pea starch granules: granule architecture of wild-type parent, r and rb single mutants, and the rrb double mutant. Carbohydr. Res. 338 (20), 2135–2147.
Rosa, M.F., Chiou, B.S., Medeiros, E.S., Wood, D.F., Mattoso, L.H.C., Orts, W.J., Imam, S.H., 2009. Biodegradable composites based on starch/evoh/glycerol blends and coconut fibers. J. Appl. Polym. Sci. 111 (2), 612–618.
Saini, J.K., Saini, R., Tewari, L., 2015. Lignocellulosic agriculture wastes as biomass feedstocks for second-generation bioethanol production: concepts and recent developments. Biotech 5 (4), 337–353.
Satyanarayana, K.G., Arizaga, G., Wypych, F., 2009. Biodegradable composites based on lignocellulosic fibers–An overview. Prog. Polym. Sci. 34 (9), 982–1021.
Sekhar, D., 2017. Mechanical properties of waste paper/jute fabric reinforced polyester resin matrix hybrid composites. Carbohydr. Polym. 172, 60–67.
Shi, H.X., Hao, Y.Y., Fang, H.Y., Xiong, Z., 2011. Separation and purification of amylose and amylopectin from cassava starch and content determination by dual-wavelength spectrophotometry. Food Sci. (N. Y.) 46 (2), 115–125.
Siracusa, V., Ingrao, C., Giudice, A.L., Mbohwa, C., Rosa, M.D., 2014. Environmental assessment of a multilayer polymer bag for food packaging and preservation: an LCA approach. Food Res. Int. 62, 151–161.
Thakur, V.K., Thakur, M.K., Gupta, R.K., 2014. Review: raw natural fiber-based polymer composites. Int. J. Polym. Anal. Char. 19, 256–271.
Vroman, I., Tighzert, L., 2009. Biodegradable polymers. Materials 2, 307–344.
Wattanakornsiri, A., Tongnunui, S., 2014. Sustainable green composites of thermoplastic starch and cellulose fibers. Songklanakarin J. Sci. Technol. 36 (2), 149–161.
Wilcox, C., van Sebille, E., Hardesty, D., 2015. Threat of plastic pollution to seabirds is global, pervasive, and increasing. Proc. Natl. Acad. Sci. Unit. States Am. 112 (38), 11899–11904.
Wilpiszewska, K., Spychaj, T., 2011. Ionic liquids: media for starch dissolution, plasticization and modification. Carbohydr. Polym. 86 (2), 424–428.
Xu, Y.Z., Soloway, R.D., Lin, X.F., Zhi, X., Weng, S.F., Wu, Q.G., Shi, J.S., Sun, W.X., Zhang, T.X., Wu, J.G., Xu, D.F., Xu, G.X., 2000. Fourier transform infrared (FTIR) mid-IR spectroscopy separates normal and malignant tissue from the colon and stomach. Gastroenterology 118 (4). A1417–A1417.
Yang, Y., Liu, C., Chang, P.R., Chen, Y., Anderson, D.P., Stumborg, M., 2010. Properties and structural characterization of oxidized starch/PVA/α-zirconium phosphate composites. J. Appl. Polym. Sci. 115 (2), 1089–1097.
Zhang, C.W., Li, F.Y., Li, J.F., Wang, L.M., Xie, Q., Xu, J., Chen, S., 2017. A new biodegradable composite with open cell by combining modified starch and plant fibers. Mater. Des. 120, 222–229.